KINETIC STUDY ON THE $Ca(OH)_2/CaO$ THERMOCHEMICAL ENERGY STORAGE SYSTEM WITH POTASSIUM NITRATE DOPING

Tao Wang, Changying Zhao *, Jun Yan

Institute of Engineering Thermophysics, Shanghai Jiao Tong University, Shanghai, China

Abstract

Thermochemical heat storage is a novel technique with high heat storage density and capable of large-scale energy storage for a long time. $Ca(OH)_2$ is a low-cost and readily available material with great application prospects, especially in the solar thermal power generation because of the suitable heat storage temperature. In this paper, KNO_3 doped $Ca(OH)_2$ was prepared by mechanical and solution mixing, and the effect of KNO_3 doping on $Ca(OH)_2/CaO$ heat storage process was studied to compare with pure $Ca(OH)_2$. Kinetic parameters and governing equations of dehydration process for pure $Ca(OH)_2$ and KNO_3 doped $Ca(OH)_2$ were obtained, which lay the foundation for the subsequent design and simulation of heat storage system. Results have shown that 10 wt% of KNO_3 doping can most effectively reduce the reaction temperature and accelerate the heat storage process with very small loss of heat storage density. It has been verified that the theoretical reaction data obtained by the kinetic control equation agrees well with the experimental data. The cycling test of the pure $Ca(OH)_2/CaO$ system and KNO_3 doped $Ca(OH)_2/CaO$ system was investigated, which reveals the failure process of the KNO_3 doped $Ca(OH)_2/CaO$. Moreover, the corresponding strategy for suppressing material failure was given.

Keywords: Thermochemical heat storage, Dehydration temperatures, $Ca(OH)_2$, Doping, Kinetic, Cycling test,

1. Introduction

With the development of society, the shortage of fossil energy has become an increasingly serious problem which promotes the development of renewable energy and energy-saving technologies. Solar thermal utilization and industrial waste heat recovery technology have become the hotspot of current research. However, the discontinuity and uneven distribution of solar energy and industrial waste heat have hindered their use. Thermal energy storage technology is an important means to achieve solar heat utilization, industrial waste heat recovery and carbon reduction (Miró et al., 2016; Prieto et al., 2016; Zhang et al., 2016). Compared with sensible heat and latent heat storage, thermochemical heat storage has a larger heat storage density and capability of long-term heat storage and the long-distance transportation of mass heat. It is a novel heat storage technology which is receiving more and more attention (Carrillo et al., 2019).

The $Ca(OH)_2/CaO$ system in this paper is a thermochemical heat storage system which has a wide range of sources, thus it is particularly suitable for high temperature heat storage (Xia et al., 2019). The reaction equation is shown in Eq.(1). (Coats and Redfern, 1964). In the heat storage process, calcium hydroxide is heated and decomposed into calcium oxide and water vapor. In the heat release process, calcium oxide reacts with water vapor to form calcium hydroxide.

$$Ca(OH)_2 \rightleftharpoons CaO + H_2O \qquad \Delta H = 104.4\text{kJ mol}^{-1} \qquad \text{(eq. 1)}$$

For $Ca(OH)_2/CaO$ system, many researchers have done fruitful research (Dai et al., 2018; Sakellariou et al., 2017; Schaube et al., 2013). However, the low heat storage rate of dehydration process is a serious problem which hinders the promotion of $Ca(OH)_2/CaO$ system. To solve this problem, some active additives were added. Kariya et al. (2016) embedded vermiculite in $Ca(OH)_2$ and found that the reaction rate of the composite material was enhanced. Yan and Zhao (2016) studied the heat storage and release process of $Ca(OH)_2/CaO$ system in a fixed bed with Li doping, and the heat storage process was accelerated. Furthermore, some salts, such as acetates and chlorides were added to lower the dehydration temperature (Shkatulov and Aristov, 2015). However, the effects of these additives on the kinetic parameters of heat storage reaction are still unclear, which are essential for the design of the heat storage system, and

© 2019. The Authors. Published by International Solar Energy Society
Selection and/or peer review under responsibility of Scientific Committee
doi:10.18086/swc.2019.22.08 Available at http://proceedings.ises.org

the relevant reaction controlling kinetic equations have not been obtained. Therefore, it is vital to obtain the decomposition kinetic parameters and governing equations for these novel composite materials after adding additives.

There are already some kinetic researches of pure $Ca(OH)_2$/CaO system, which have obtained the kinetic parameters of pure $Ca(OH)_2$/CaO system under different conditions, and the mechanism of the heat storage reaction is figured out(Criado et al., 2014; Long et al., 2017; Schaube et al., 2012). In our previous work, Yan and Zhao (2014, 2015) calculated the energy barrier of dehydration from $Ca(OH)_2$ to CaO according to the first principle theory, and founded that after doping with Li, the energy barrier in dehydration process becomes lower, which means the same heat storage efficiency can be achieved at a lower temperature with Li doping. They also used the differential method and integral method to obtain the decomposition kinetic equations of pure $Ca(OH)_2$ and $Ca(OH)_2$ after Li doping.

Since K and Li belong to the same main group in the periodic table and K is close to the position of Ca, this paper used the inexpensive and easily available additive, KNO_3, to study the dehydration process of doped $Ca(OH)_2$. The thermodynamic properties and kinetic parameters of the composites were obtained and compared with pure $Ca(OH)_2$, which provided a theoretical basis for the design and simulation of the $Ca(OH)_2$/CaO heat storage system. In addition, the cycling stability of the doped material was also investigated.

2. Experimental setup

2.1 Material preparation

In order to study the effect of KNO_3 on the $Ca(OH)_2$/CaO heat storage system, three different doping ratios of KNO_3-$Ca(OH)_2$ composite heat storage materials were prepared, the mass ratio of KNO_3 was 5%, 10% and 25%, respectively. Both KNO_3 and $Ca(OH)_2$ were purchased from Sinopharm Chemical Reagent Co., Ltd, Shanghai, China. The main chemical composition of the samples is shown in Tab. 1.

Tab. 1: Chemical composition and characteristics of the commercial $Ca(OH)_2$ and KNO_3

Materials	Composition			
$Ca(OH)_2$	$Ca(OH)_2$≥95.0%	Mg, alkali metal ≤0.5%	NH_4OH≤0.25%	Sulfate≤0.2%
KNO_3	KNO_3≥99.0%	Mg, alkali metal ≤0.26%	NH_4OH≤0.001%	Sulfate≤0.003%

The details and procedures of KNO_3 doping are shown as follows. Agate mortar was used in the initial mechanical mixing process. The total sample mass was strictly controlled at 6 g in each mechanical mixing process, so the weight of KNO_3 required for different samples can be calculated based on the mass fraction. Therefore, the mass of KNO_3 in each mechanical mixing was 0.3 g, 0.6 g, and 1.5 g, respectively, while the corresponding $Ca(OH)_2$ mass was 5.7 g, 5.4 g, and 4.5 g, respectively. KNO_3 and $Ca(OH)_2$ were mechanically ground in an agate mortar for 10 min. Then the premixed sample was transferred to a 50 ml beaker and added 20 ml distilled water. The mixture was stirred at a constant temperature of 90 °C for 1.5 h using a thermostatic stirrer manufactured by Shanghai Yangyingpu Instrument & Meter Manufacturing Co., Ltd. After the completion of the heating, the mixture was dried at 120 °C for 3 h using a vacuum drying oven (Shanghai Yiheng Scientific Instrument Co., Ltd.) to obtain the KNO_3-$Ca(OH)_2$ composite material. The prepared KNO_3-$Ca(OH)_2$ composite material was named as CH-N, the composite material after CH-N dehydration was named as C-N, where N is the mass fraction of KNO_3.

2.2 Material characterization

In order to study the effect of KNO_3 on the heat storage process of $Ca(OH)_2$/CaO heat storage system，the non-isothermal decomposition experiment was carried out using the DSC8000 Differential Scanning Calorimeter of PerkinElmer. In the experiment, the sample weight was controlled between 9.1 and 9.8 mg in each test, the sample was heated from 100 °C to 550 °C at the heating rate of 15 °C min^{-1}. High-purity nitrogen (99.999%) was used as the purge gas with the gas flow rate of 20 ml min^{-1} in the experiment. The muffle furnace (SX2-5-12, Shanghai Tianye Electric Furnace Factory Co., Ltd, Shanghai, China) was used to test the effect of KNO_3 on heat storage rate, three grams of CH-10 and pure $Ca(OH)_2$ were placed in the muffle furnace, and weighed every few minutes until the sample was completely decomposed.

In order to study the effect of KNO_3 on the failure process of KNO_3 doped $Ca(OH)_2$, the morphologies of samples with different cycle times were characterized by using scanning electron microscope (SEM, Nova NanoSEM 230 instrument, USA, FEI). XRD test was also performed on samples with different cycle times. Diffraction data was collected by step scanning using a step size of 0.02 °, a scan step time of 1 s, and a scan range of 5 °-60 ° 2θ.

2.3 Non-isothermal kinetics characterization

In order to obtain the kinetic equation and parameters of the dehydration process, the non-isothermal dehydration test was carried out using the STA8000 synchronous thermal analyzer of PerkinElmer. The sample weight was controlled between 7.2 and 7.6 mg in each test; the initial temperature was set at 150 °C, then the sample was heated to 600 °C at the heating rate of 2.5 °C min^{-1}, 5 °C min^{-1}, 10 °C min^{-1} and 15 °C min^{-1}, respectively. Besides, high purity argon was used as purge gas with the gas flow rate of 20 ml min^{-1} in the test.

3 Kinetic calculation of dehydration process

3.1 Non-isothermal kinetics of the dehydration process

According to the concept of reaction order raised by Van't Hoff and various rate constant relations of Arrhenius (Vyazovkin et al., 2011), the governing equation representing the non-isothermal reaction kinetics can be obtained, which is shown in Eq. (2).

$$\frac{\mathrm{d}\alpha}{\mathrm{d}T}=(\frac{A}{\beta})\exp(-\frac{E}{RT})f(\alpha) \qquad \text{(eq. 2)}$$

Where, α is the conversion rate of the dehydration process, namely molar fraction reacted, which can be calculated by using Eq. (3); T is the thermodynamic temperature; the constants include A, β, E, R. A is the pre-exponential factor; β is the heating rate; E is the apparent activation energy; R is the molar gas constant; $f(\alpha)$ is the mechanism function of reaction kinetics.

$$\alpha=\frac{m_{\mathrm{ini}}-m_{\mathrm{s}}}{m_{\mathrm{ini}}\times w_{\mathrm{ch}}}\times\frac{M_{\mathrm{ch}}}{M_{\mathrm{H_2O}}} \qquad \text{(eq. 3)}$$

Where, m_{ini} is the initial weight of sample, m_{s} is the sample weight in real time, w_{ch} is the mass ratio of $Ca(OH)_2$, M_{ch} is the molecular weight of $Ca(OH)_2$ while $M_{\mathrm{H_2O}}$ is the molecular weight of H_2O.

The relationship between $d\alpha/dt$ and $\exp(-1/T)$ according to Eq. (2) for dehydration process of pure $Ca(OH)_2$ and KNO_3 doped $Ca(OH)_2$ is shown in Fig. 1 and Fig. 2 respectively. The model method was used to get more accurate kinetic parameters, and the activation energy E, pre-exponential factor $\ln A$ and mechanism function were calculated using the non-isothermal experiment.

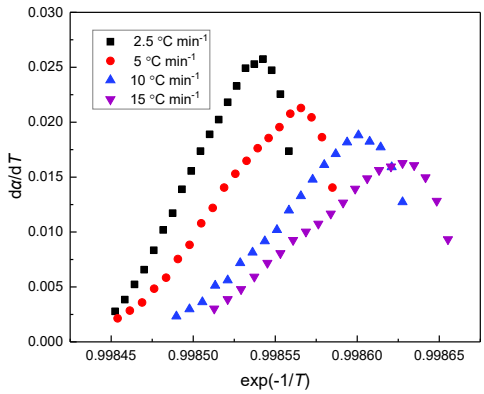

Fig. 1: The relationship between $d\alpha/dt$ and $\exp(-1/T)$ for dehydration process of pure $Ca(OH)_2$

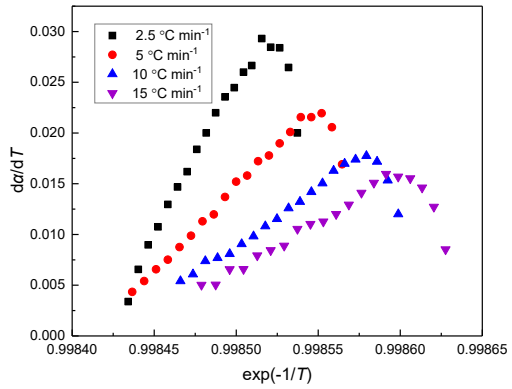

Fig. 2: The relationship between dα/dt and exp(-1/T) for dehydration process of CH-10

3.2 Calculation procedure of the model method and error analysis

The Coats–Redfern integral method (Coats and Redfern, 1964) and the Achar–Brindly–Sharp (ABS) differential method (Achar et al., 1966) were used to obtain the kinetic parameters.

Coats–Redfern method

$$\ln\frac{g(\alpha)}{T^2}=\ln(\frac{AR}{\beta E})-\frac{E}{RT} \qquad \text{(eq. 4)}$$

ABS method

$$\ln\frac{\mathrm{d}(\alpha)}{f(\alpha)\mathrm{d}T}=\ln(\frac{A}{\beta})-\frac{E}{RT} \qquad \text{(eq. 5)}$$

Where $g(\alpha)$ and $f(\alpha)$ are the reaction kinetic mechanism function in integral and differential forms, respectively.

The linear fitting method was used to fit the data calculated by non-isothermal experiment, where the left side of Eq. (4) and Eq. (5) was regarded as ordinate, and the $1/T$ was chosen as the abscissa. According to the non-isothermal experiment data and the reaction mechanism function above, the activation energy and pre-exponential factor can be obtained from the intercept and slope of the fitting straight line. Three different reaction mechanism functions were used to obtain the most suitable kinetic parameters, which are listed in Tab. 2. In order to ensure the accuracy of the kinetic parameters, the thermogravimetric experiment results at the heating rate of 5 °C min^{-1}, 10 °C min^{-1} and 15 °C min^{-1} were adopted in the kinetic calculation, while the experiment result at the heating rate of 2.5 °C min^{-1} was used to check the calculated kinetic equation.

Tab. 2: Three reaction mechanism functions of gas-solid reaction mechanisms.

Reaction model	Code	$g(\alpha)$	$f(\alpha)$
Mample (first order)	F_1	$-\ln(1-\alpha)$	$(1-\alpha)$
Contracting cylinder	R_2	$1-(1-\alpha)^{1/2}$	$2(1-\alpha)^{1/2}$
One-dimensional diffusion	D_1	α^2	$(1/2)\alpha^{-1}$

The error analysis process is as follows, the system error can be calculated using Eq. (6).

$$u_s=\sqrt{\left(\frac{\partial h}{\partial T}\bullet u(T)\right)^2+\left(\frac{\partial h}{\partial \alpha}\bullet u(\alpha)\right)^2} \qquad \text{(eq. 6)}$$

Where, the weight inaccuracy is 0.0001 mg for electronic balance of the TGA and the temperature inaccuracy is 0.01 °C for the TGA. Therefore, $u(\alpha)$ is ±0.0013%; and $u(T)$ is ±0.0025%.

The error of the activation energy (E) can be calculated using Eq. (7).

$$u_E=\sqrt{(u_s)^2+(u_{f1})^2} \qquad \text{(eq. 7)}$$

Where the u_{f1} is the fitting error of the apparent activation energy.

The error of the ln$A$ can be calculated by Eq. (8) for the Coats-Redfern method and Eq. (9) for ABS method.

$$u_{\ln A}=\sqrt{(u_E)^2+(u_{f2})^2} \qquad \text{(eq. 8)}$$

$$u_{\ln A} = u_{f2} \quad \text{(eq. 9)}$$

Where the u_{f2} is the fitting error of ln$A$.

As a result, the error of activation energy is nearly 2.64%-4.32% for the Coats-Redfern method and 2.76%-6.52% for the ABS method, while the error of ln$A$ is about 2.96%-5.17% for the Coats-Redfern method and 2.13%-5.90% for the ABS method.

4. Results and discussion

4.1 Influence of KNO_3 on the heat storage process

According to the DSC signal of endothermic dehydration process of pure $Ca(OH)_2$ and samples with different doping ratios, the onset temperature and heat storage density were calculated, the results are listed in Tab. 3. When doped with 5% KNO_3, the onset temperature of the reaction reduces from 461.43 °C to 446.48 °C, as the mass fraction of KNO_3 rises from 5% to 10%, the onset temperature of the dehydration reaction drops by approximately 15 K. However, when the mass fraction rises from 10% to 25%, the reaction onset temperature only drops by nearly 7 K, that is, with the increase of the mass fraction, the onset temperature of the reaction rapidly decreases. When the mass fraction of KNO_3 exceeds 10%, the reaction onset temperature decreases at a slower rate. Considering that the heat storage density of the composite material cannot be reduced too much, 10 wt% is the optimal addition ratio of KNO_3. At this ratio, the onset temperature of the dehydration reaction can be effectively reduced, (approximately 32 K), and the reduction of the heat storage density of the composite material can also be ignored.

Tab. 3: The onset temperature and heat storage density of dehydration reaction for pure $Ca(OH)_2$ and KNO_3 doped $Ca(OH)_2$

Materials	Onset temperature (°C)	Heat storage density (kJ kg^{-1})
CH	461.43	1435.16
CH-5	446.80	1365.25
CH-10	428.49	1317.06
CH-25	421.78	1096.56

As shown in Fig. 3, the decomposition process of CH-10 took only 45 minutes while the decomposition process of pure $Ca(OH)_2$ took almost 80 minutes, which means the decomposition rate of CH-10 is almost twice that of pure $Ca(OH)_2$. Therefore, doping KNO_3 can effectively increase heat storage rate and regulate heat storage temperature.

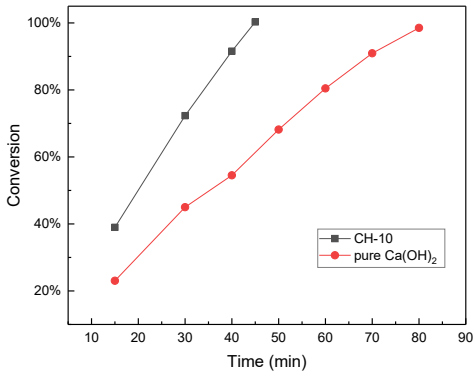

Fig. 3: The heat storage process of pure $Ca(OH)_2$ and CH-10 in muffle furnace

4.2 Verification of the composition of CH-10

In order to evaluate the composition of CH-10, XRD test was performed. The XRD pattern is shown in Fig. 4. In Fig. 4(a), XRD pattern of pure $Ca(OH)_2$ shows that the major phase is portlandite ($Ca(OH)_2$), while the calcite phase ($CaCO_3$) can also be observed. The calcite phase can be regarded as the impurity. In Fig. 4 (b), for CH-10, reflexes of low intensity from KNO_3 can be detected, and this can prove that KNO_3 has been doped into $Ca(OH)_2$.

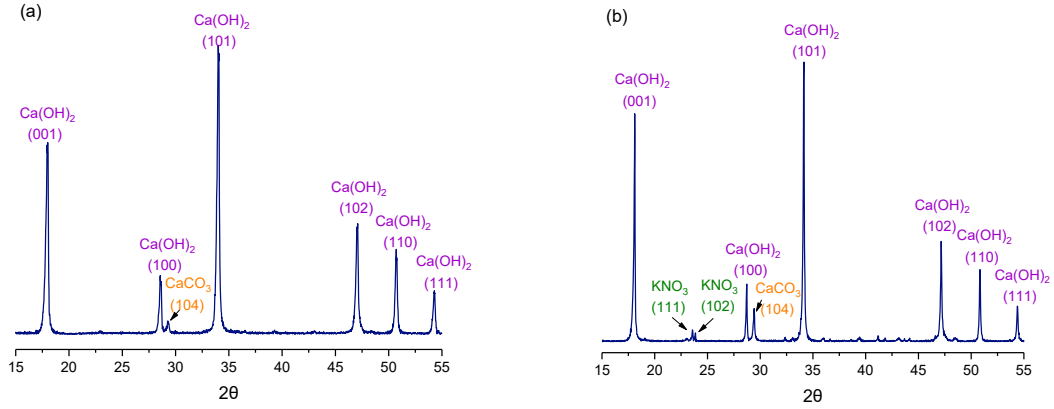

Fig. 4: XRD pattern of pure $Ca(OH)_2$ (a) and CH-10 (b)

4.3 Kinetics of pure $Ca(OH)_2$

In the light of the model fitting process and the R-Square results in Tab. 4, the F_1 model is the most suitable reaction model for the dehydration process of pure $Ca(OH)_2$. Besides, it is also the closest model between the integral and the differential method. The kinetic parameters are listed in Tab. 5. After averaging the integral results and the differential results, the final activation energy E and pre-exponential factor A for the dehydration of pure $Ca(OH)_2$ are 7.6×10^4 J mol^{-1} and 9.81×10^8 s^{-1}, respectively. Thus, the kinetic equation can be expressed as Eq. (10).

$$\frac{d\alpha}{dt} = (9.81\times10^8)\times\exp(-\frac{7.6\times10^4}{RT})\times(1-\alpha) \qquad \text{(eq. 10)}$$

Tab. 4: R-Square results of model fitting process (for pure $Ca(OH)_2$)

Reaction model	Rs of Coats-Redfern (mean)	Rs of ABS (mean)
F_1	0.9900	0.9938
R_2	0.9622	0.9704
D_1	0.9489	0.9349

Tab. 5: Kinetic parameters calculated by Coats-Redfern and ABS method (for pure $Ca(OH)_2$)

β	Coats-Redfern			ABS			Model
	E (J mol^{-1})	ln$A$	Rs	E (J mol^{-1})	ln$A$	Rs	
5	9.0×10^4	25	0.98883	7.5×10^4	21	0.99116	F1
10	8.5×10^4	23	0.99142	6.9×10^4	19	0.99541	F1
15	7.6×10^4	20	0.98975	6.1×10^4	16	0.99495	F1
Mean	8.4×10^4	22.8	-	6.8×10^4	18.5	-	

4.4 Kinetics of CH-10

The calculation of kinetic parameters reflects that the F_1 model has the best fitting result for the dehydration process of CH-10 according to Tab. 6. The kinetic parameters are shown in Tab. 7. The integral results and the differential results were averaged to obtain the final kinetic parameters, the activation energy E and pre-exponential factor A for the dehydration of CH-10 are 6.4×10^4 J mol^{-1} and 5.94×10^7 s^{-1}, respectively. Thus, the kinetic equation can be expressed as Eq. (11).

$$\frac{d\alpha}{dt} = (5.94\times10^7)\times\exp(-\frac{6.4\times10^4}{RT})\times(1-\alpha) \qquad \text{(eq. 11)}$$

Tab. 6: R-Square results of model fitting process (for CH-10)

Reaction model	Rs of Coats-Redfern (mean)	Rs of ABS (mean)
F_1	0.9868	0.9936
R_2	0.9749	0.9868
D_1	0.9622	0.9622

Tab. 7: Kinetic parameters calculated by Coats-Redfern and ABS method (for CH-10)

β	Coats-Redfern			ABS			Model
	E (J mol^{-1})	ln$A$	Rs	E (J mol^{-1})	ln$A$	Rs	
5	8.4×10^4	24	0.98113	6.5×10^4	19	0.99348	F1
10	7.0×10^4	19	0.99010	5.2×10^4	14	0.99370	F1
15	6.6×10^4	18	0.98930	4.9×10^4	13	0.99361	F1
Mean	7.3×10^4	20.5	-	5.5×10^4	15.3	-	

4.5 Verification of the kinetic control equation for pure $Ca(OH)_2$ and CH-10

In order to check the validity of the derived kinetic equations, the thermogravimetric data at the heating rate of 2.5 °C min^{-1} was compared with the theoretical data calculated by using Eq. (10) and Eq. (11), as well as the heating rate β. As shown in Fig. 5 and Fig. 6, whether it is pure $Ca(OH)_2$ or CH-10, the theoretically calculated data is in good agreement with the actual measured data, and the growth trend is consistent. Therefore, the kinetic equation can be utilized in subsequent simulation for fixed bed.

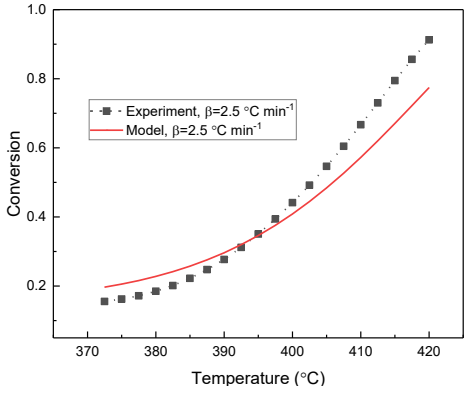

Fig. 5: Comparison of theoretical and experimental results for pure $Ca(OH)_2$ dehydration process

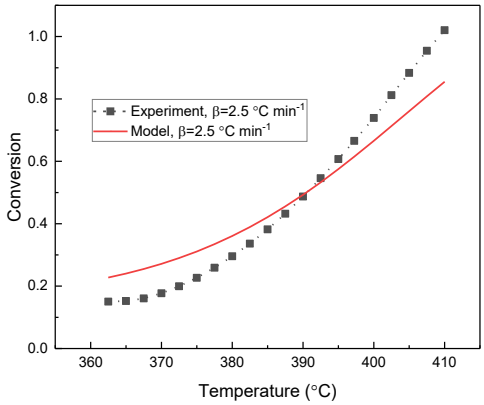

Fig. 6: Comparison of theoretical and experimental results for CH-10 dehydration process

4.6 Comparison of kinetics between CH-10 and pure $Ca(OH)_2$

As shown in Fig. 7, the apparent activation energy will be reduced approximately 1.2×10^4 J mol^{-1} after doping KNO_3, which means that the dehydration process can be accomplished more easily with KNO_3 doping and a higher

heat storage efficiency can be achieved at the same temperature. In addition, this can explain the reduction of onset temperature and the increase of heat storage rate after KNO_3 doping.

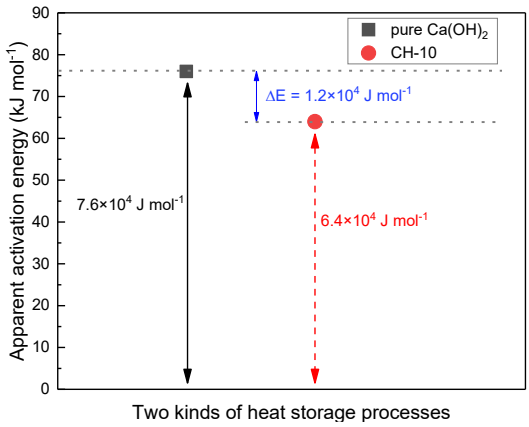

Fig. 7: Apparent activation energy reduction caused by KNO_3 doping

4.7 The cycling test of pure $Ca(OH)_2$

Fig. 8 and Fig. 9 show the SEM images of pure $Ca(OH)_2$ and CaO at different cycling stages. Initially, the microstructures of pure $Ca(OH)_2$ and CaO are loose networks like wisps of cotton wool. However, as the cycle progresses, the microstructures of pure $Ca(OH)_2$ and CaO become compact and irregular spheres. As shown in Fig. 10, with the cycle progressing, the corresponding peak intensity of $CaCO_3$ is growing, indicating that the proportion of material failure is gradually increasing.

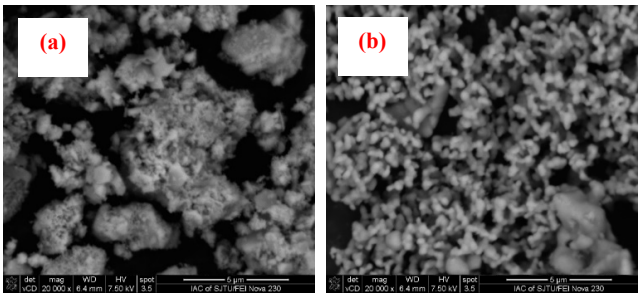

Fig. 8: Pure $Ca(OH)_2$ SEM images of different cycles ((a) cycle 1; (b) cycle 25)

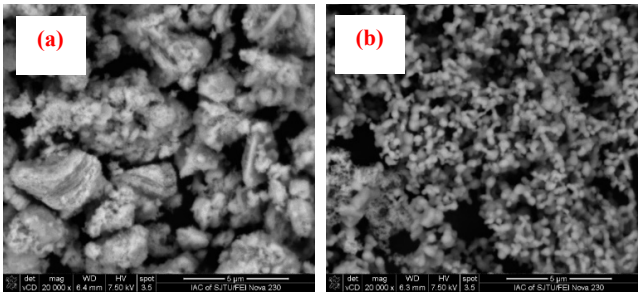

Fig. 9: Pure CaO SEM images of different cycles ((a) cycle 1; (b) cycle 25)

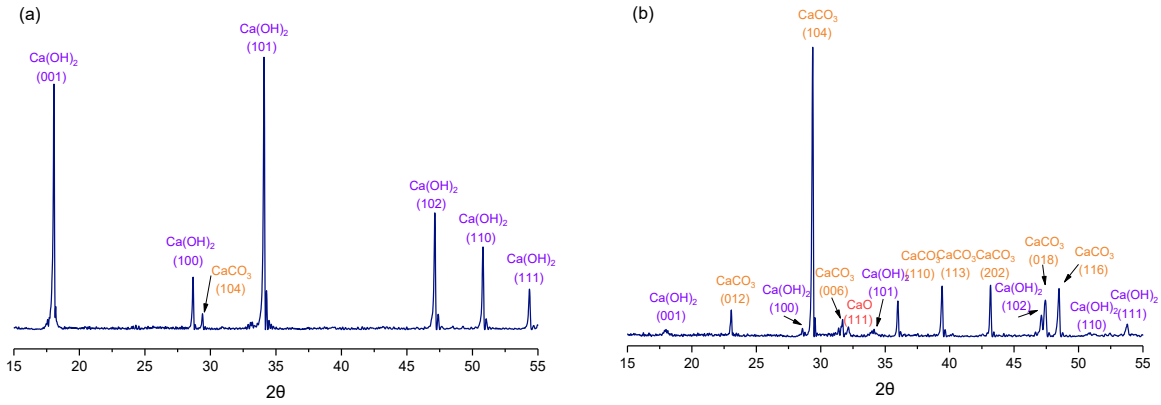

Fig. 10: XRD pattern of pure $Ca(OH)_2$ with different cycles ((a) cycle 1; (b) cycle 25)

4.8 The cycling test of CH-10

Fig. 11 and Fig. 12 show the SEM images of CH-10 and C-10 at different cycling stages. It is worth noting that, unlike the heat storage and exothermic processes of pure $Ca(OH)_2/CaO$, the morphology of C-10 produced by CH-10 dehydration is blocky rather than loose network structure. Moreover, when C-10 hydrates to CH-10, the block structure is as if being torn apart, then eventually grows into a flower-like structure, which means that the specific surface area of the material is increased. When CH-10 dehydrates into C-10, the flower-like structure shrinks and eventually becomes a blocky structure. Undoubtedly, the addition of KNO_3 makes the $Ca(OH)_2$ become a flower-like structure during the hydration process, which can enhance the heat and mass transfer. Therefore, the promotion of dehydration of CH-10 by KNO_3 is manifested in two aspects. On the one hand, it reduces the activation energy of the reaction, on the other hand, KNO_3 regulates the morphology of the material in the heat storage and exothermic reaction, which promotes heat and mass transfer.

According to Fig. 13, the peak of KNO_3 still exists after 25 cycles, indicating that the failure of the material is completely due to carbonation, and KNO_3 has good stability during the cycle. For CH-10, evacuating the reactor before the heat storage and releasing process to insulate CO_2 from the heat storage material is a recommended method to inhibit carbonation. In addition, the cyclic stability of CH-10 after evacuating the reactor needs to be further studied.

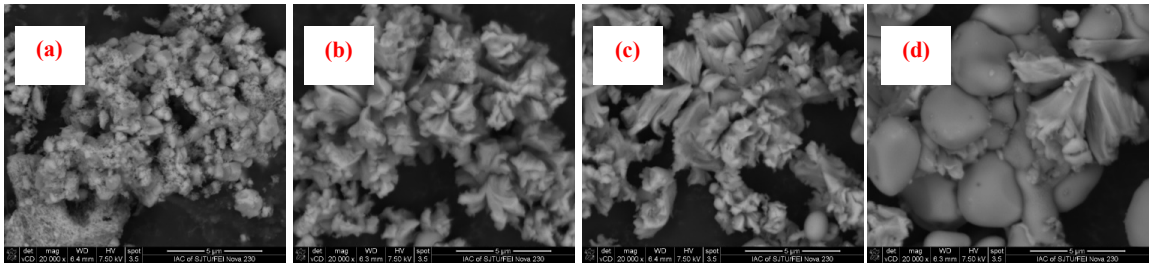

Fig. 11: CH-10 SEM images of different cycles ((a) cycle 1; (b) cycle 5; (c) cycle 10; (d) cycle 25)

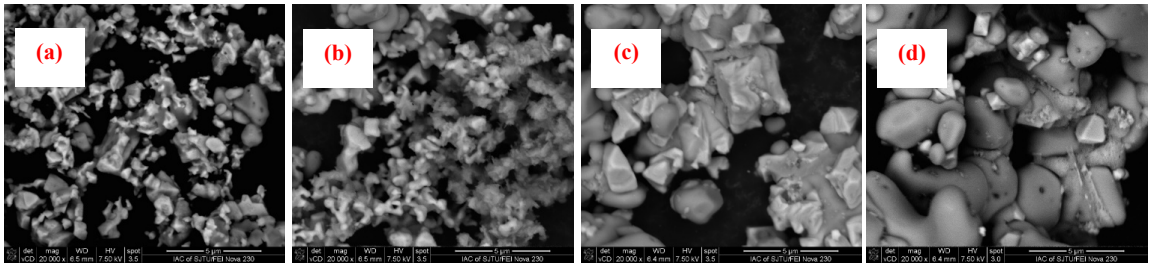

Fig. 12: C-10 SEM images of different cycles ((a) cycle 1; (b) cycle 5; (c) cycle 10; (d) cycle 25)

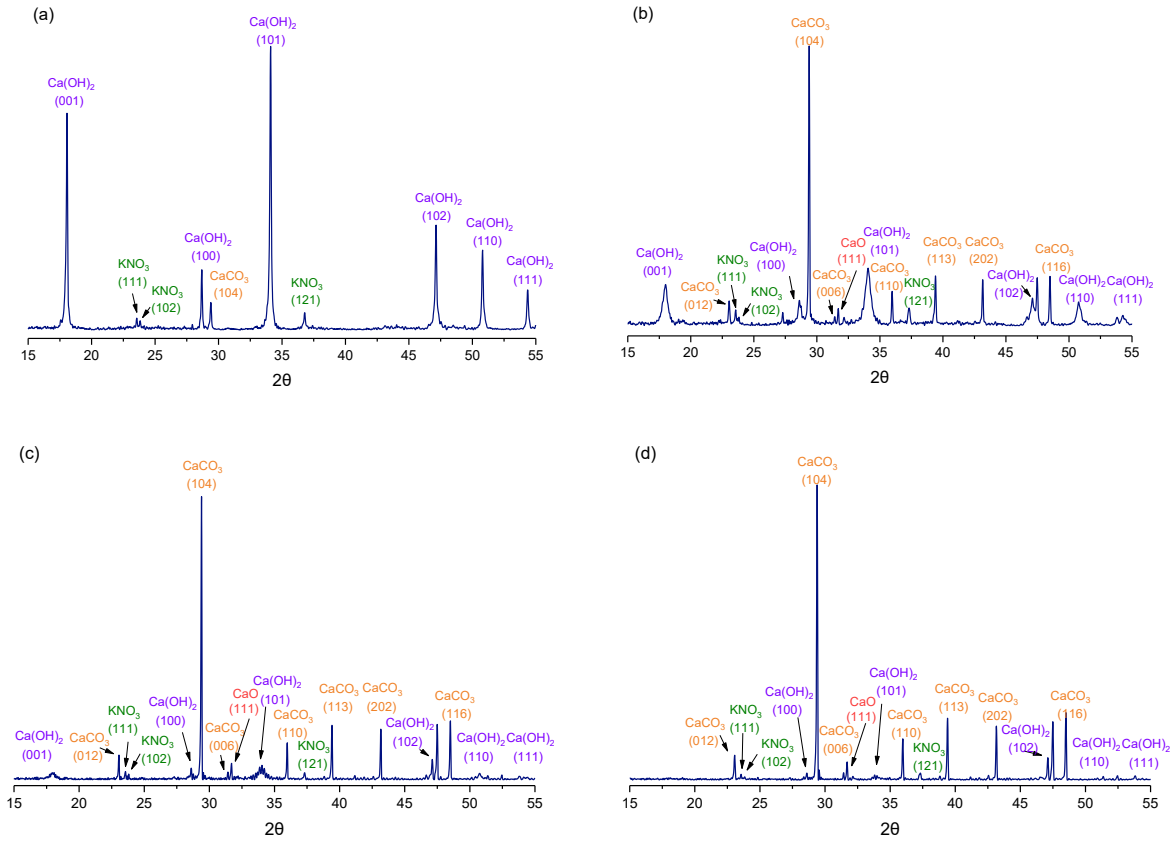

Fig. 13: XRD pattern of CH-10 with different cycles ((a) cycle1; (b) cycle5; (c) cycle 10; (d) cycle 25)

5 Conclusions

The KNO_3 doped $Ca(OH)_2$ is a promising TCES material with great reaction performance. KNO_3 doping will reduce the heat storage temperature and evidently increase the heat storage rate. Therefore, KNO_3-doped $Ca(OH)_2$/CaO heat storage system can be used for lower temperature heat storage, its operating temperature range can be broadened. The kinetic parameters and corresponding control equations of pure $Ca(OH)_2$ and KNO_3 doped $Ca(OH)_2$ were obtained. KNO_3 doping can effectively reduce apparent activation energy, which promotes the heat storage reaction. For the cycling test analysis, unlike pure $Ca(OH)_2$, there is a flower-like microstructure in KNO_3 doped $Ca(OH)_2$ during cycling, which reinforces the heat and mass transfer processes and promotes the heat storage reaction accordingly. The XRD pattern shows that KNO_3 has good cycling stability, which means it can still work after 25 cycles.

6. Acknowledgments

This work is supported by the National Natural Science Foundation of China (Grant No. 51706130).

7. References

1. Achar, B.N., Brindley, G.W., Sharp, J.H., Kinetics and mechanism of dehydroxylation process. III. Applications and limitations of dynamic methods. In: Proceedings of International Clay Conference Jerusalem, 1966, 1: 67–73.
2. Carrillo, A.J., Gonzalez-Aguilar, J., Romero, M., Coronado, J.M., 2019. Solar Energy on Demand: A Review on High Temperature Thermochemical Heat Storage Systems and Materials. Chem Rev 119(7), 4777-4816.
3. Coats, A.W., Redfern, J.P., 1964. Kinetic parameters from thermogravimetric data. Nature 201 (4914), 68–69.
4. Criado, Y.A., Alonso, M., Abanades, J.C., 2014. Kinetics of the CaO/$Ca(OH)_2$ Hydration/Dehydration Reaction for Thermochemical Energy Storage Applications. Industrial & Engineering Chemistry Research 53(32), 12594-12601.
5. Dai, L., Long, X.-F., Lou, B., Wu, J., 2018. Thermal cycling stability of thermochemical energy storage system $Ca(OH)_2$/CaO. Applied Thermal Engineering 133, 261-268.
6. Kariya, J., Ryu, J., Kato, Y., 2016. Development of thermal storage material using vermiculite and calcium hydroxide. Applied Thermal Engineering 94, 186-192.
7. Long, X.F., Dai, L., Lou, B., Wu, J., 2017. The kinetics research of thermochemical energy storage system $Ca(OH)_2$/CaO. International Journal of Energy Research 41(7), 1004-1013.
8. Miró, L., Gasia, J., Cabeza, L.F., 2016. Thermal energy storage (TES) for industrial waste heat (IWH) recovery: A review. Applied Energy 179, 284-301.
9. Prieto, C., Cooper, P., Fernández, A.I., Cabeza, L.F., 2016. Review of technology: Thermochemical energy storage for concentrated solar power plants. Renewable and Sustainable Energy Reviews 60, 909-929.
10. Sakellariou, K.G., Criado, Y.A., Tsongidis, N.I., Karagiannakis, G., Konstandopoulos, A.G., 2017. Multi-cyclic evaluation of composite CaO-based structured bodies for thermochemical heat storage via the CaO/$Ca(OH)_2$ reaction scheme. Solar Energy 146, 65-78.
11. Schaube, F., Koch, L., Wörner, A., Müller-Steinhagen, H., 2012. A thermodynamic and kinetic study of the de- and rehydration of $Ca(OH)_2$ at high H_2O partial pressures for thermo-chemical heat storage. Thermochimica Acta 538, 9-20.
12. Schaube, F., Kohzer, A., Schütz, J., Wörner, A., Müller-Steinhagen, H., 2013. De- and rehydration of $Ca(OH)_2$ in a reactor with direct heat transfer for thermo-chemical heat storage. Part A: Experimental results. Chemical Engineering Research and Design 91(5), 856-864.
13. Shkatulov, A., Aristov, Y., 2015. Modification of magnesium and calcium hydroxides with salts: An efficient way to advanced materials for storage of middle-temperature heat. Energy 85, 667-676.
14. Vyazovkin, S., Burnham, A.K., Criado, J.M., Pérez-Maqueda, L.A., Popescu, C., Sbirrazzuoli, N., 2011. ICTAC Kinetics Committee recommendations for performing kinetic computations on thermal analysis data. Thermochimica Acta 520(1-2), 1-19.
15. Xia, B.Q., Pan, Z.H., Yan, J., Zhao, C.Y., 2019. Mesoscopic exploration on mass transfer in porous thermochemical heat storage materials. International Journal of Heat and Mass Transfer 135, 52-61.
16. Yan, J., Zhao, C.Y., 2014. First-principle study of CaO/$Ca(OH)_2$ thermochemical energy storage system by Li or Mg cation doping. Chemical Engineering Science 117, 293-300.
17. Yan, J., Zhao, C.Y., 2015. Thermodynamic and kinetic study of the dehydration process of CaO/$Ca(OH)_2$ thermochemical heat storage system with Li doping. Chemical Engineering Science 138, 86-92.
18. Yan, J., Zhao, C.Y., 2016. Experimental study of CaO/$Ca(OH)_2$ in a fixed-bed reactor for thermochemical heat storage. Applied Energy 175, 277-284.
19. Zhang, H., Baeyens, J., Cáceres, G., Degrève, J., Lv, Y., 2016. Thermal energy storage: Recent developments and practical aspects. Progress in Energy and Combustion Science 53, 1-40.